Damping and decoherence of Fock states in a nanomechanical resonator due to two-level systems

Laura G. Remus and Miles P. Blencowe
Department of Physics and Astronomy, Dartmouth College, Hanover, New Hampshire 03755, USA
(Received 30 June 2012; revised manuscript received 19 September 2012; published 15 November 2012)

We numerically investigate the decay of initial quantum Fock states and their superpositions for a mechanical resonator mode coupled to an environment comprising interacting, damped tunneling two-level system (TLS) defects. The cases of one, three, and six near-resonant, interacting TLS's are considered in turn, and it is found that, with even as few as three TLS's, the resonator's quantum decay behavior is indistinguishable from that due to coupling to an Ohmic oscillator bath.

DOI: 10.1103/PhysRevB.86.205419 PACS number(s): 85.85.+j, 03.65.Yz

I. INTRODUCTION

The quest to understand the quantum-to-classical transition has led to the development of macroscopic mechanical systems in which researchers hope to realize quantum states. In a 2010 landmark experiment,[1] a state corresponding to a single quantum of vibrational energy in a mechanical resonator was created and its subsequent decay dynamics measured. We anticipate that similar measurements involving a higher number quantum Fock states and their superpositions in a mechanical system will be achieved in the near future. In light of these developments, there is a need to understand the quantum state decay mechanisms that enforce classicality in these systems.

In the early 1970s, an explanation was provided for the observed anomalous thermal behavior of amorphous materials at cryogenic temperatures by invoking the existence of tunneling two-level system (TLS) defects that couple via their elastic dipole moments to phonons.[2,3] Subsequent acoustic phonon pulse attenuation, acoustic hole burning, and acoustic phonon pulse echo experiments provided strong confirming evidence for the existence of interacting TLS's in these materials.[4–8] More recently, the relevance of TLS defects for micron-scale superconducting qubit dynamics was established, where the TLS's are thought to reside in the tunnel barrier oxide layer and in the substrate, and couple via their electric dipole moments to the qubits.[9–19]

The same amorphous materials are often used in the fabrication of nanoscale to micron-scale mechanical systems, and thus it is likely that TLS's will play a significant role in their quantum-to-classical transition at cryogenic temperatures.[20–24] In particular, we anticipate that TLS's will provide one of the main mechanisms for the decay of quantum states in mechanical resonators (even though such an understanding comes with a lack of a clear microscopic picture of what actually constitutes a TLS defect). In Ref. 25, we presented an estimate indicating that a given low-order flexural mode of a micron-scale mechanical resonator vibrating at radio frequencies may be near resonance with a few TLS's, but is unlikely to interact resonantly with large numbers of TLS's. These TLS's couple to the motion of the resonator via its strain, and thus will be part of the environment responsible for the decay of quantum flexural modes. Reference 25 numerically investigated the damping of initially coherent states and the decoherence dynamics of initial superpositions of spatially separated coherent states, where the environment consisted of either one or three damped TLS's. Clear signatures of resonator amplitude dependence were observed in the damping dynamics, a consequence of TLS saturation. This behavior is qualitatively different from the amplitude-independent damping of initial coherent states resulting from the standard, Ohmic oscillator bath model of an environment.

However, it is of interest to explore the damping and decoherence dynamics for other types of initial, quantum resonator states, such as Fock states and their superpositions. We have in mind experiments involving high-frequency nanoscale to micron-scale mechanical resonators that are cryogenically cooled to low temperatures, such as for Ref. 1. In the aforementioned experiment, mechanical Fock states were prepared and measured by using an electromechanically coupled, superconducting phase qubit that was controllably tuned into and out of resonance with the mechanical resonator mode. We would like in particular to establish whether probing Fock state decay can distinguish between the mechanical resonator flexural mode coupling predominantly to a bath comprising a few near-resonant TLS's and to a phonon bath describing elastic radiation loss through the resonator supports.[26]

In this work, we numerically model the low-temperature ($k_BT \ll \hbar\omega$) damping and decoherence dynamics of a mechanical resonator coupled to between one and six damped TLS's that are near-resonant with the resonator, where the latter is initially prepared in either a single Fock state or a superposition of Fock states. We find, perhaps surprisingly, that the damping and decoherence dynamics is practically indistinguishable from that resulting from coupling to an Ohmic oscillator bath, even with only three near-resonant damped TLS's furnishing the mechanical resonator environment. In particular, the Fock state decay rate is observed to scale closely as n, where n is the initial number of resonator quanta (Fock state number), while the decoherence time of a superposition of ground and excited Fock states is found to be close to twice the decay time of the excited state, coinciding with the Ohmic model trends. A partial understanding of these numerical results can be obtained from a simpler, Born-Markov approximated master equation model for the resonator subsystem that treats perturbatively the coupling between the resonator and damped TLS's to second order (with the latter traced over as the bath) and which facilitates analytical calculations for the decay times. However, even more surprising is the observation that completely removing the TLS's damping does

not alter the Ohmic damping/decoherence-like behavior for the resonator subsystem, even though the Born-Markov master equation model is no longer valid. The latter observation is reminiscent of recent numerical investigations to establish subsystem thermalization of closed, interacting many-body quantum systems;[27] in our case, the single oscillator mode system itself induces interactions between the many TLS's.

In the next section, we present our model system-environment master equation, with a more detailed derivation given in Ref. 25. Section III investigates the damping dynamics of Fock states and decoherence dynamics of superpositions of Fock states for a mechanical resonator coupled to first a single TLS, then three near-resonant TLS's, and finally six near-resonant TLS's, where direct interactions between the TLS's are neglected. An approximate master equation model is presented, yielding analytical decay rate expressions that partially explain the numerically observed trends. In Sec. IV, we begin by deriving the oscillator-TLS Hamiltonian with pairwise interactions between TLS's mediated via the resonator's strain field. The effect of TLS-TLS interactions on the damping of Fock states and decoherence of Fock state superpositions in a resonator coupled to first three and then six near-resonant, interacting TLS's is investigated. Finally, we offer some concluding remarks in Sec. V.

II. RESONATOR-TLS SYSTEM EQUATIONS

In this section, we present the model for the resonator-TLS. For the TLS Hamiltonian, we have

$$\hat{H}_{\rm TLS} = \sum_{\alpha=1}^{N}\left[\frac{1}{2}\Delta_0^{(\alpha)}\sigma_z^{(\alpha)} + \frac{1}{2}\Delta_b^{(\alpha)}\sigma_x^{(\alpha)}\right], \tag{1}$$

where $\alpha = 1,2,\ldots,N$ labels the TLS, $\Delta_0^{(\alpha)}$ is the asymmetry of the αth TLS's potential well, and $\Delta_b^{(\alpha)}$ is its tunnel splitting that depends on the well barrier height and width. Writing out the resonator mode–TLS Hamiltonian, we have

$$\hat{H}_S = \hbar\omega(a^\dagger a + 1/2) + \sum_{\alpha=1}^{N}\left[\frac{1}{2}\Delta_0^{(\alpha)}\sigma_z^{(\alpha)} + \frac{1}{2}\Delta_b^{(\alpha)}\sigma_x^{(\alpha)} + \lambda^{(\alpha)}(a+a^\dagger)\sigma_z^{(\alpha)}\right], \tag{2}$$

where $a^\dagger$ and a are raising and lowering operators for the resonator mode of interest, satisfying the commutation relation $[a,a^\dagger] = 1$. The resonator mode–TLS coupling $\lambda^{(\alpha)}$ arises from the mechanical elastic strain dependence of the TLS asymmetry energy. The elastic strain for a given resonator mode is spatially dependent and hence the coupling $\lambda^{(\alpha)}$ depends on the location of the given αth TLS defect within the resonator. A detailed derivation of the coupling for the example of the fundamental mode of a long, thin elastically isotropic mechanical beam is given in Ref. 25. Note that the Hamiltonian (2) neglects interactions between the TLS's beyond those induced via the system's single oscillator mode; pairwise interactions between the TLS's induced by the mechanical resonator's elastic strain field will be considered below in Sec. IV.

In Ref. 25, we derive the following master equation describing the dissipative dynamics of the coupled resonator-TLS system:

$$\begin{aligned}\dot{\rho}_S(t) = &-\frac{i}{\hbar}[H_S,\rho_S(t)] - \frac{i\gamma}{2\hbar}[Y,\{P_Y,\rho_S(t)\}] \\ &- \frac{m\omega\gamma}{2\hbar}\coth\left(\frac{\hbar\omega}{2k_BT}\right)[Y,[Y,\rho_S(t)]] \\ &- \sum_{\alpha=1}^{N}\frac{1}{4T_1^{(\alpha)}}\left(\frac{E^{(\alpha)}}{\Delta_b^{(\alpha)}}\right)^2\left[\sigma_z^{(\alpha)},\left[\sigma_z^{(\alpha)},\rho_S(t)\right]\right] \\ &- \sum_{\alpha=1}^{N}\frac{i}{4T_1^{(\alpha)}}\left(\frac{E^{(\alpha)}}{\Delta_b^{(\alpha)}}\right)\tanh\left(\frac{E^{(\alpha)}}{2k_BT}\right) \\ &\times\left[\sigma_z^{(\alpha)},\left\{\sigma_y^{(\alpha)},\rho_S(t)\right\}\right],\end{aligned} \tag{3}$$

where $\rho_S(t)$ is the resonator-TLS system density matrix, $Y = Y_{zp}(a+a^\dagger)$ gives the mechanical resonator mode displacement (with Y_{zp} the zero-point displacement uncertainty), P_Y is the resonator mode momentum, and $E^{(\alpha)} = \sqrt{(\Delta_0^{(\alpha)})^2 + (\Delta_b^{(\alpha)})^2}$ is the αth TLS energy level separation. The parameter γ gives the energy damping rate of the oscillator resulting from coupling to a bath of oscillators with Ohmic spectral density (modeling, e.g., clamping loss). We will restrict ourselves for the most part to the effect of the damped TLS's only on the mechanical resonator, considering nonzero γ only when comparing with the effect on a mechanical resonator of a pure Ohmic oscillator bath. The parameter $T_1^{(\alpha)}$ gives the αth TLS relaxation time from its excited energy eigenstate in the absence of the oscillator. We shall use dimensionless time units, $t \to \omega t$, with T_1 and γ expressed as ωT_1 and γ/ω, respectively, and λ, Δ_i, and temperature T expressed as $\lambda/\hbar\omega$, $\Delta_i/\hbar\omega$, and $k_BT/\hbar\omega$, respectively.

In the following sections, we solve the master equation (3) numerically using the QUANTUM OPTICS TOOLBOX[28] for up to $N = 6$ TLS's and for resonator initial Fock states $|n\rangle$ and their superpositions with $n \leqslant 10$. The resonator state space dimension was truncated at $n_{\rm cutoff} = 35$, which was found to provide more than adequate convergence for the quantum dynamics. We shall use somewhat larger than typical material values for the oscillator-TLS coupling strength λ in order to have manageable numerical integration times.

III. DAMPING AND DECOHERENCE DUE TO NONINTERACTING TLS's

A. Single TLS

In this section, we investigate the damping of Fock states and the decoherence of Fock state superpositions in a mechanical resonator interacting with a single damped TLS. As a partial check of our numerical methods, we begin by evaluating the number state probability $P_n = \langle n|\rho|n\rangle$ as a function of time for a resonator mode coupled to an Ohmic oscillator bath only, where the analytical solution is known. Figure 1 shows the log of the number state probability for initial Fock states $|n\rangle$, with $n = 0$ to 11, when there is an Ohmic oscillator bath only. (Note that all logarithms are to base e.) The slope of each successive curve decreases by an increment of $1/T_{11}$, where T_{11} is the lifetime of the first excited state; as expected, the number state lifetime decays as $1/n$.[29]

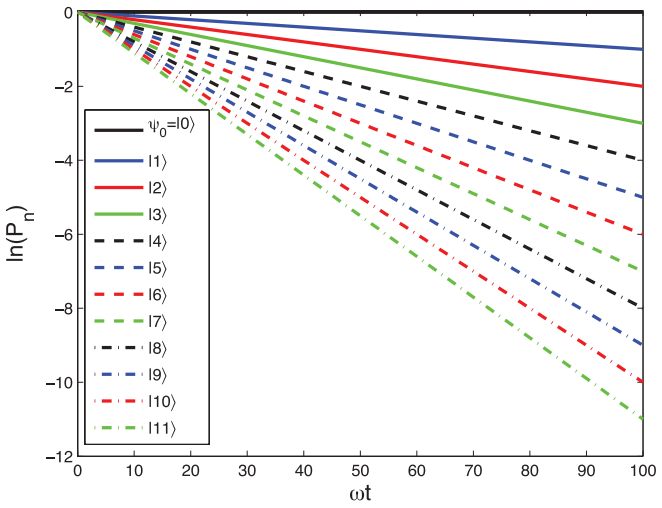

FIG. 1. (Color online) Natural log of number state probability P_n vs ωt for a range of initial Fock states for the resonator coupled to an Ohmic oscillator bath only, where $\gamma = 0.01$ and $T = 0.09$.

Figure 2 shows the number state probability for the resonator coupled to a single, on-resonance damped TLS. In this case, we see that the P_n curves oscillate, as energy is transferred from the resonator to the TLS and back. As a partial check of the numerics, the time of the first minimum of each curve for $n \geqslant 1$ corresponds closely to the Jaynes-Cummings model prediction for the transfer time of a quantum of vibrational energy to a symmetric, on-resonance TLS: $\omega t = \pi E/(2\lambda\sqrt{n})$, where $\hbar\omega = E = \Delta_b$. The left-hand plot shows the number state probability for four low-n states and the right-hand plot for three high-n states. The high-n states appear to decay at close to the same rate, as indicated by the black curve, which follows the maxima of the oscillating probabilities; the same black curve is shown for comparison in the left-hand plot, and in this case the P_n plots clearly fall short of this "maximum" curve, appearing to signify more rapid decay than the indicated high-n states. These trends are clearly qualitatively different from the Ohmic oscillator bath case discussed above, where the decay rate increases linearly with n.

Next, we investigate the effect of a damped TLS on number state superpositions. A useful "visual" representation of the state is its Wigner function, defined in terms of the mechanical resonator mode displacement Y and momentum P_Y as[30]

$$W(Y,P_Y) = \frac{1}{h}\int d\xi\, e^{-iP_Y\xi/\hbar}\langle Y+\xi/2|\rho|Y-\xi/2\rangle d\xi. \qquad (4)$$

Figure 3 shows two initial oscillator states: an equal mixture of the ground and $n = 7$ state [Fig. 3(a)], and a superposition of the same two Fock states [Fig. 3(b)]. In both cases, the Wigner function has positive and negative values, because both the Fock state mixture and the superposition are nonclassical states. However, the spokelike interference fringes in the superposition plot indicate the presence of nonzero off-diagonal terms of the density matrix, as opposed to the concentric undulations in the mixture plot. Figure 4 shows four equally spaced interval snapshots of the Wigner function for a resonator initially in the superposition state shown in Fig. 3(b). The resonator is coupled to an Ohmic bath that causes the state to decay and the amplitude of the Wigner function to decrease. However, both the ring and spokelike structures of the initial state are still visible in the final snapshot. Figure 5 shows a similar set of snapshots, this time for a resonator coupled to an on-resonance, damped TLS only. In contrast to the superposition state decay in the Ohmic bath case, we see that the spokelike structure disappears first, leaving concentric rings similar to those seen in Fig. 3(a). The dephasing time T_ϕ is usually defined in terms of the decay times of the on- and off-diagonal terms of the resonator's density matrix as follows:

$$\frac{1}{T_{0n}} = \frac{1}{2T_{nn}} + \frac{1}{T_\phi}, \qquad (5)$$

where T_{0n} is the lifetime of the off-diagonal density matrix element ρ_{0n}, and T_{nn} is the lifetime of the diagonal matrix element ρ_{nn}. The disappearance of the spokes prior to the rings suggests a finite T_ϕ, in contrast to an oscillator bath, where $T_{0n} = 2T_{nn}$.

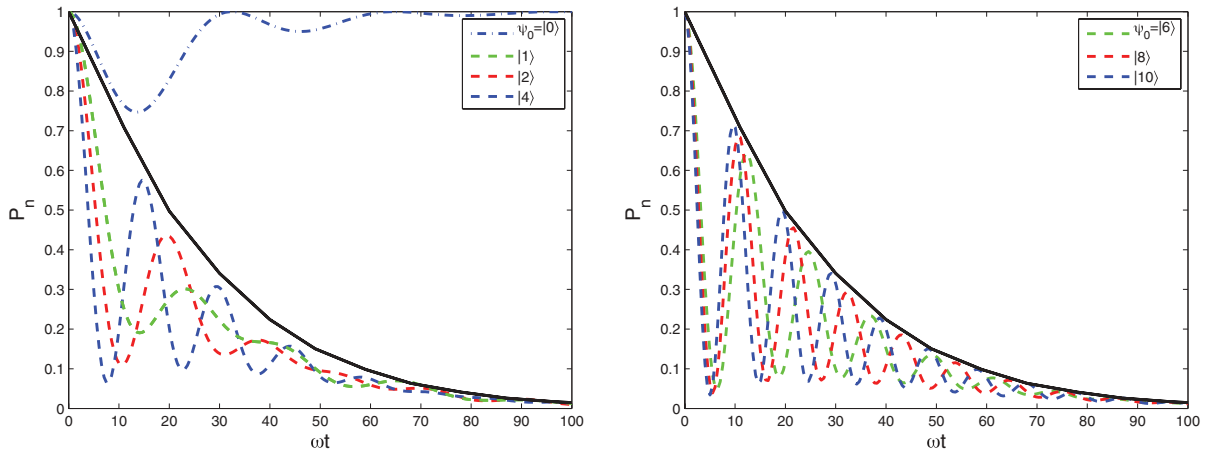

FIG. 2. (Color online) Number state probability P_n vs ωt for various initial Fock states for the resonator coupled to a damped TLS only. The black curve, indicating the peaks of the curves in the right-hand plot, is the same in both plots. For both plots, $\Delta_0 = 0$, $\Delta_b = 1$, $\lambda = 0.1$, $T = 0.09$, and $T_1 = 10$.

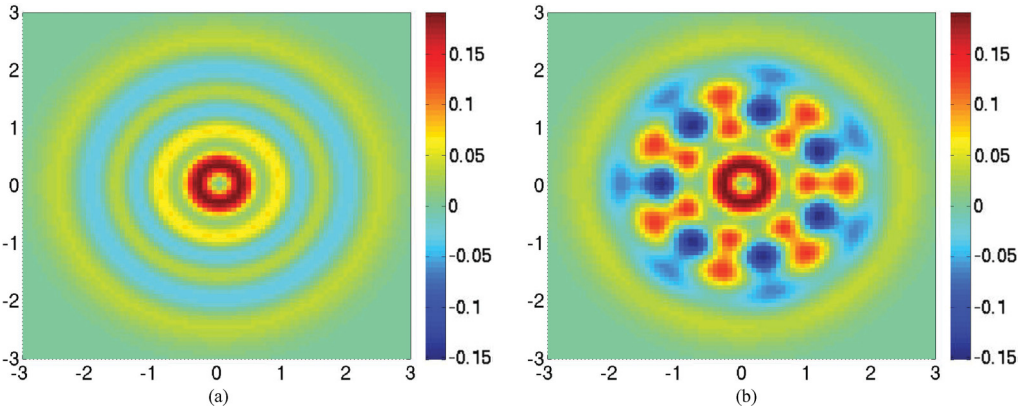

FIG. 3. (Color online) Wigner function for a mixture of number states $|0\rangle$ and $|7\rangle$ (a) and for a superposition of the same states (b). The horizontal and vertical axes are dimensionless mechanical resonator position Y/Y_{zp} and momentum $P_Y/(m\omega Y_{zp})$, respectively.

B. Three TLS's

We now increase the number of damped TLS's to three. The TLS energies $\Delta_0^{(\alpha)}$ and $\Delta_b^{(\alpha)}$, $\alpha = 1,2,3$, are chosen randomly according to the standard tunneling model (STM) distribution.[8,25] As our condition for near resonance, the corresponding TLS energies $E^{(\alpha)}$ are restricted to the range $0.75\hbar\omega \leqslant E^{(\alpha)} \leqslant 1.25\hbar\omega$, where recall that $E^{(\alpha)} = \sqrt{(\Delta_0^{(\alpha)})^2 + (\Delta_b^{(\alpha)})^2}$. We also choose random values for the $T_1^{(\alpha)}$ relaxation times of each individual TLS by first selecting a reference T_1 value and then assigning to each TLS a randomly generated $T_1^{(\alpha)}$ within $\pm 50\%$ of the reference value. Furthermore, each TLS is assigned a random $\lambda^{(\alpha)}$ coupling that is within $\pm 50\%$ of a reference value $\lambda = 0.1/6$, scaled down from the single TLS coupling considered in the previous section ($\lambda = 0.1$) so as to avoid significant TLS-induced renormalizations of the resonator's harmonic potential resulting from having more coupled TLS's. We choose a temperature $T = 0.09$ for all plots.

To investigate Fock state decay, we choose an initial state $|\psi_0\rangle = |n\rangle$ and then determine the corresponding number state probability P_n as a function of time. Figure 6 shows the decay of P_n for a range of initial Fock states. Note that there is a small numerical integration error that manifests itself in the ground state $|0\rangle$ probability rising slightly above 1 over the integration time $\omega t = 100$. However, this error is sufficiently small as to have a negligible effect on the Fock state decay dynamics for $n \geqslant 1$. In contrast to the single-TLS case, the number state probabilities do not show large oscillations but instead decay relatively smoothly. Furthermore, the nearly linear curves in the log plot indicate that P_n decays exponentially and the decay rates can be extracted from a linear fit. We noted in the previous section that for a resonator damped by an Ohmic bath, the decay time for the nth state goes as $T_{nn} = T_{11}/n$, where T_{11} is the decay time for the first excited state: the decay rate scales as n. Figure 7 shows the normalized decay rate T_{11}/T_{nn} for P_n as a function of n. For a resonator coupled solely to an Ohmic bath, the curve has a slope equal to 1. For a resonator coupled to three TLS's, the slope is very close to 1; Fock states decay similarly to a resonator that is Ohmically coupled to a bath of free oscillators.

We now investigate the decay of a superposition of the ground state and the nth excited state, $|\psi\rangle = 1/\sqrt{2}(|0\rangle + |n\rangle)$, with each TLS initially in a thermal state. We consider the ρ_{nn} and ρ_{0n} elements of the density matrix as a function of time (plots not shown). The curves decay approximately exponentially; we apply a linear fit to the log of the curves to find the diagonal and off-diagonal decay times, T_{nn} and T_{0n}, respectively. Figure 8 shows the log of the decay times as a function of $\ln(n)$ for a range of T_1 values. We plot $2T_{nn}$ to allow for a comparison to the relation $T_{0n} = 2T_{nn}$ for an Ohmic bath. The curves in Fig. 8 all decay uniformly and with a slope ≈ -1. The $2T_{nn}$ and T_{0n} curves are very similar: dephasing is negligible compared to decay.

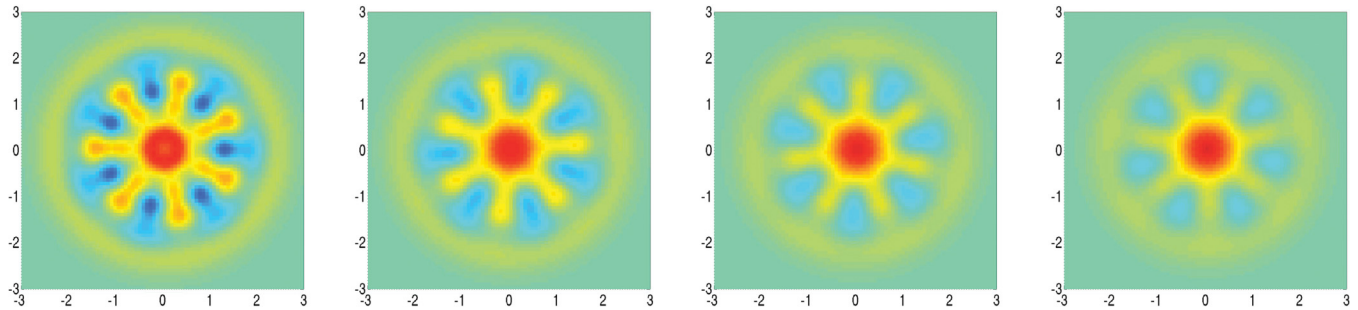

FIG. 4. (Color online) Evolving Wigner function for the resonator initially in the superposition state shown in Fig. 3(b) coupled to an Ohmic oscillator bath with $\gamma = 0.01$ and $T = 0.09$.

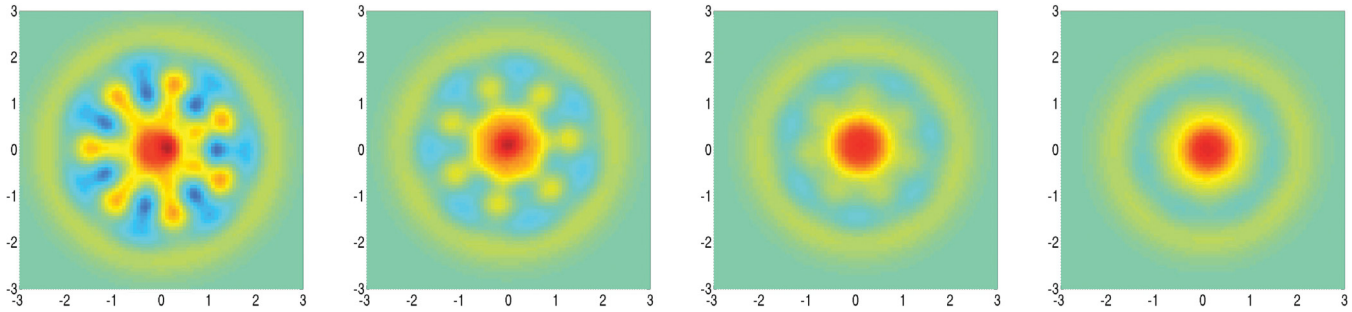

FIG. 5. (Color online) Evolving Wigner function for the resonator initially in the superposition state shown in Fig. 3(b) coupled to a damped TLS with $\lambda = 0.1, \Delta_0 = 0, \Delta_b = 1, T = 0.09$, and $T_1 = 10$.

The curves in Fig. 8 show a surprising dependence on T_1. As a reminder, $T_1^{(\alpha)}$ is the decay time of the αth TLS from its excited to ground state. Because T_1 determines the strength of the coupling between a TLS and its bath, with smaller T_1 corresponding to stronger coupling, we would expect T_{nn} and T_{0n} to decrease as T_1 decreases; stronger coupling would result in shorter resonator Fock state decay times. However, Fig. 8 shows that the opposite is true. The curve with $T_1 = 1$ shows longer decay times than the curve with $T_1 = 100$. The lowest (solid green) curve is for a resonator coupled to three *undamped* TLS's, and thus a T_1 for this curve is not given. This curve shows the shortest decay times, and appears to be the large-T_1 limit of the curves for the damped TLS's.

To further investigate the T_1 dependence of the decay times, in Fig. 9 we plot T_{0n} and $2T_{nn}$ as a function of T_1 for the $n = 4$ superposition state. The plot shows a strong dependence on T_1, particularly for $T_1 < 10$, and suggests that reducing the TLS-bath coupling causes superposition states to decay more quickly. This surprising dependence on T_1 will be discussed in further detail below in Sec. III D. Finally, in Fig. 10 we plot $2T_{nn}$ and T_{0n} versus n for three different realizations of the randomized TLS parameters. While the curves indicate the same qualitative linear dependence $T_{nn} = T_{11}/n$, there is some scatter in the T_{11} values, as indicated by the different intercepts. This is to be expected given that we have only a small statistical sample of three randomly selected TLS's coupled to the resonator.

C. Six TLS's

We now consider a resonator coupled to six noninteracting TLS's. We assign random values to the TLS energies $\Delta_0^{(\alpha)}$ and $\Delta_b^{(\alpha)}$ according to the STM distribution, as well as random values to the resonator-TLS coupling term $\lambda^{(\alpha)}$ and the TLS $T_1^{(\alpha)}$ times, selected as in the previous section. The temperature $T = 0.09$ for all plots. We first consider the decay of a Fock state as a function of time for a resonator coupled to six damped spins. From the log plot in Fig. 11, we see that the log of the number state probability P_n decays approximately linearly with time. The oscillations at long times for the higher energy states are numerical artifacts arising from the exponentially small P_n values. We can apply a linear fit to the log plot to determine the n dependence of the decay rate. As for the resonator coupled to three TLS's, we find that the resonator's normalized decay rate scales with the initial Fock state number similarly to that of an Ohmic bath, i.e., with slope ≈ -1 (see Fig. 22).

Next, we study the decay of a superposition of the ground state and the nth excited state. Figure 12 shows the log of T_{0n} and $2T_{nn}$ versus the log of the initial n characterizing the

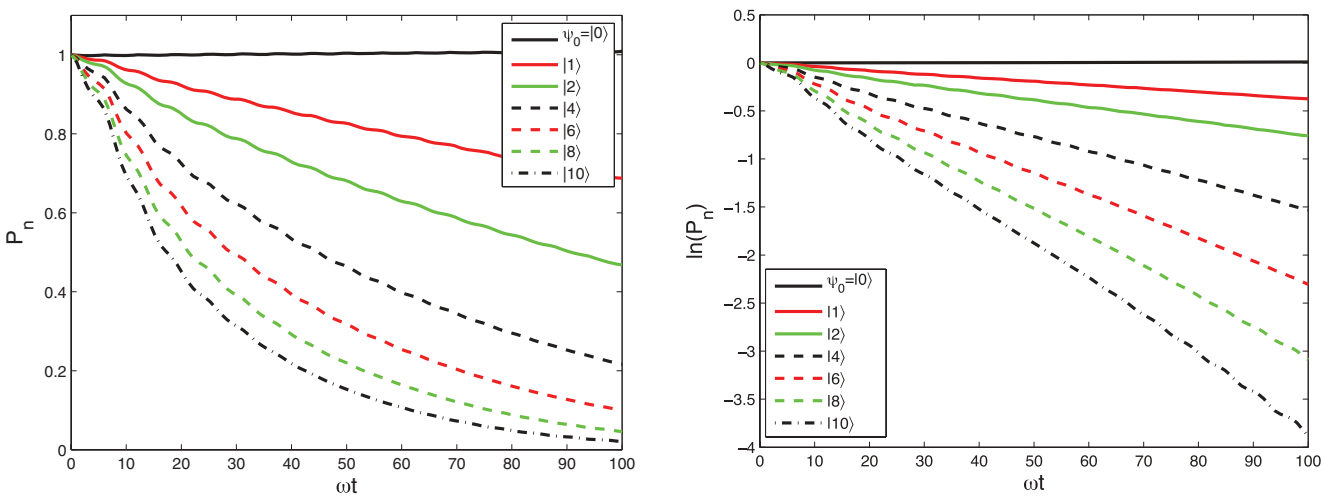

FIG. 6. (Color online) Left: P_n vs ωt for a resonator coupled to three noninteracting TLS's. Right: $\ln(P_n)$ vs ωt. For all curves, $T_1 = 10$.

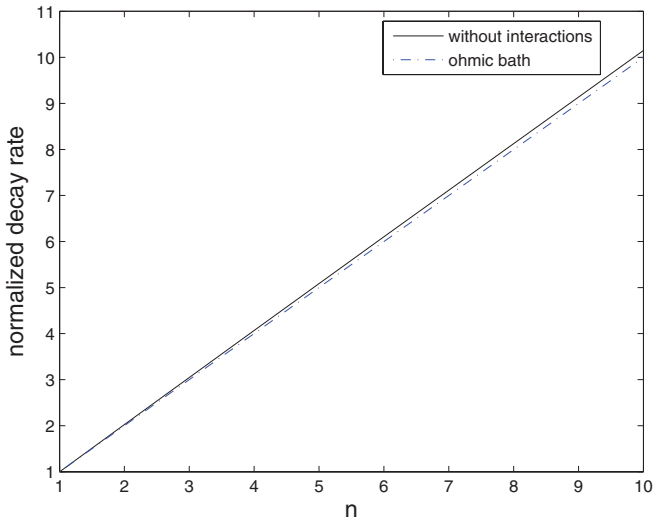

FIG. 7. Normalized decay rate vs n for single Fock states. The resonator is coupled to three noninteracting TLS's (solid) and to an Ohmic bath without any TLS's present (dot-dash). For both curves, $T_1 = 10$.

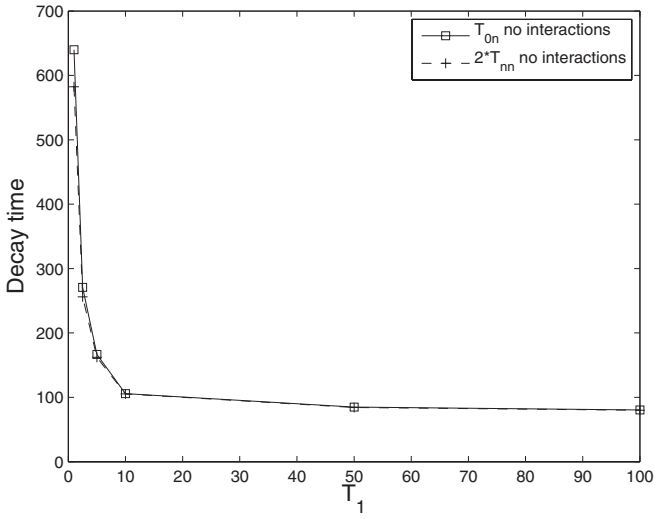

FIG. 9. $2T_{nn}$ and T_{0n} vs T_1 for the $n = 4$ superposition state. The resonator is coupled to three noninteracting TLS's.

superposition state for seven different values of the average TLS T_1 time. We note that all of the curves have a slope ≈ -1. Similar to Fig. 8 for three TLS's, Fig. 12 shows little difference between T_{0n} and $2T_{nn}$ for the different values of T_1; dephasing is negligible.

In Fig. 13, we show the T_1 dependence of the on- and off-diagonal decay times for the $n = 4$ superposition state. The plot shows the same strong dependence on T_1 as for the case of three TLS's (Fig. 9). As a reminder, T_1 is the time it takes for a TLS in its excited state to decay to its ground state. Thus, we would expect that as we decreased T_1, the resonator states would dampen more quickly, resulting in a shorter decay time. For six TLS's, however, we find that as we decrease T_1, the diagonal and off-diagonal terms of the density matrix decay more slowly. This unexpected behavior suggests that the coupling between the TLS's and their individual baths is somehow obstructing a more efficient means of dissipation. This is supported by the lowest curve in Fig. 12, which is for a resonator coupled to six TLS's that are *not* coupled to their individual baths, and yet indicates the shortest oscillator Fock state decay time. In Sec. III D, we show through an analytical approximation that this behavior can be partially explained by considering the TLS bath Lorentzian linewidth dependencies on T_1.

Finally, as we did for three noninteracting TLS's, we now plot the decay of T_{nn} and T_{0n} for three different realizations of the TLS parameters. Figure 14 shows that the groups of six TLS's exhibit a higher degree of agreement than the three-TLS groups did (Fig. 10), with uniform slopes ≈ -1. This is a good indication that we have moved to a regime more akin to a dense TLS spectrum, with variations in the parameters of individual TLS's having less of an impact on the resonator.

D. Analytical approximation to Fock state damping

In this section, we present an analysis of Fock state damping due to TLS's. We assume that the coupling between the mechanical resonator and the N TLS's is sufficiently weak

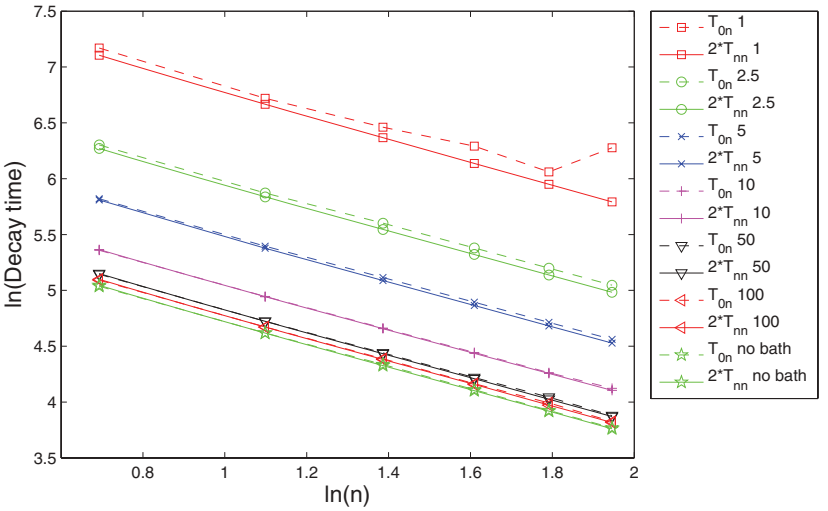

FIG. 8. (Color online) T_{0n} and $2T_{nn}$ for the initial superposition state $|\psi_0\rangle = 1/\sqrt{2}(|0\rangle + |n\rangle)$ with a range of T_1 values shown in the legend. In particular, T_1 ranges from 1 to 100, while "no bath" denotes that the TLS's are undamped. The observed trend for a given n is decreasing decay time with increasing T_1. For all curves, the resonator is coupled to three noninteracting TLS's.

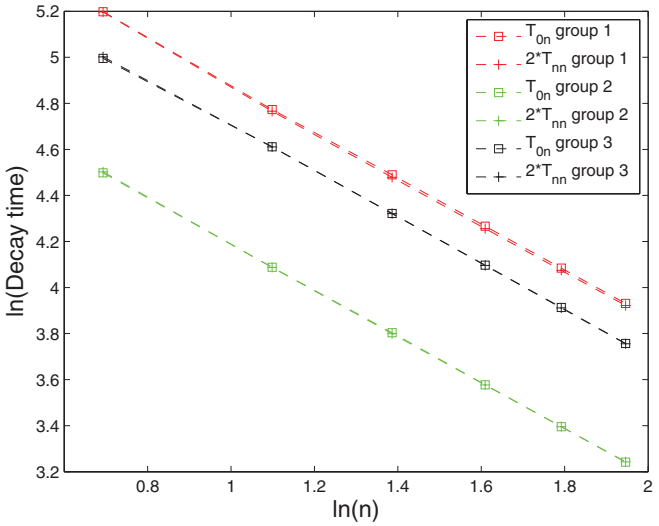

FIG. 10. (Color online) $2T_{nn}$ and T_{0n} vs n for three different groups of the TLS parameters. For all curves, $T_1 = 10$.

that we can make a self-consistent Born approximation, where we expand perturbatively to second order in the resonator-TLS couplings and trace over the TLS's to obtain the following resonator master equation:

$$\dot{\rho}_m(t) = -\frac{i}{\hbar}[H_m, \rho_m(t)] - \frac{1}{\hbar^2}\int_0^t dt' \left\{ \frac{1}{2}\langle\{B(t), B(t')\}\rangle [Y, [Y(t'-t), \rho_m(t)]] + \frac{1}{2}\langle [B(t), B(t')]\rangle [Y, \{Y(t'-t), \rho_m(t)\}] \right\}, \quad (6)$$

where ρ_m and H_m are the mechanical resonator density matrix and Hamiltonian, respectively, and

$$B(t) = \sum_{\alpha=1}^{N} \lambda^{(\alpha)} \sigma_z^{(\alpha)}(t), \quad (7)$$

with $\lambda^{(\alpha)}$ the coupling between the oscillator and the αth TLS. Solving for the TLS-environment dynamics in the absence of the resonator, one can find the symmetric $\langle\{B(t), B(t')\}\rangle$ and antisymmetric $\langle [B(t), B(t')]\rangle$ correlation functions of the TLS bath. Thus, in the above Born approximation, we neglect the influence of the resonator on the TLS dynamics. More specifically, the approximation does not account for possible nonlinear, resonator amplitude-dependent saturation effects, or the possibility of coherent energy exchange between the resonator and the TLS's. The importance of these effects depends on the relative coupling strengths between the mechanical resonator and the TLS's, and between the TLS's and their respective baths. Following the analysis in Ref. 11, we have the following for the TLS bath correlation functions:

$$\frac{1}{2}\langle\{B(t), B(t')\}\rangle = \sum_{\alpha=1}^{N} (\lambda^{(\alpha)})^2 \left[\cos^2\theta^{(\alpha)} \left(1 - \langle\sigma_z^{(\alpha)}\rangle^2\right) e^{-\Gamma_1^{(\alpha)}(t-t')} + \sin^2\theta^{(\alpha)} \cos[E^{(\alpha)}(t-t')/\hbar] e^{-\Gamma_2^{(\alpha)}(t-t')} \right] \quad (8)$$

and

$$\frac{1}{2}\langle [B(t), B(t')]\rangle = -i \sum_{\alpha=1}^{N} (\lambda^{(\alpha)})^2 \sin^2\theta^{(\alpha)} \langle\sigma_z^{(\alpha)}\rangle \times \sin[E^{(\alpha)}(t-t')/\hbar] e^{-\Gamma_2^{(\alpha)}(t-t')}, \quad (9)$$

where $\langle\sigma_z^{(\alpha)}\rangle = \tanh[E^{(\alpha)}/(k_B T)]$, $\sin\theta^{(\alpha)} = \Delta_b^{(\alpha)}/E^{(\alpha)}$, and $\cos\theta^{(\alpha)} = \Delta_0^{(\alpha)}/E^{(\alpha)}$. The TLS dephasing rate is given in terms of the relaxation rate as

$$\Gamma_2^{(\alpha)} = \left[\frac{1}{2} + \left(\frac{\Delta_0^{(\alpha)}}{\Delta_b^{(\alpha)}} \right)^2 \right] \Gamma_1^{(\alpha)}, \quad (10)$$

where $\Gamma_1^{(\alpha)} = T_1^{(\alpha)-1}$. We now substitute Eqs. (8) and (9) into the mechanical resonator master equation (6), and we insert the free resonator (oscillator) dynamics solution

$$Y(t'-t) = Y_{zp}(a e^{-i\omega_m(t'-t)} + a^\dagger e^{i\omega_m(t'-t)}). \quad (11)$$

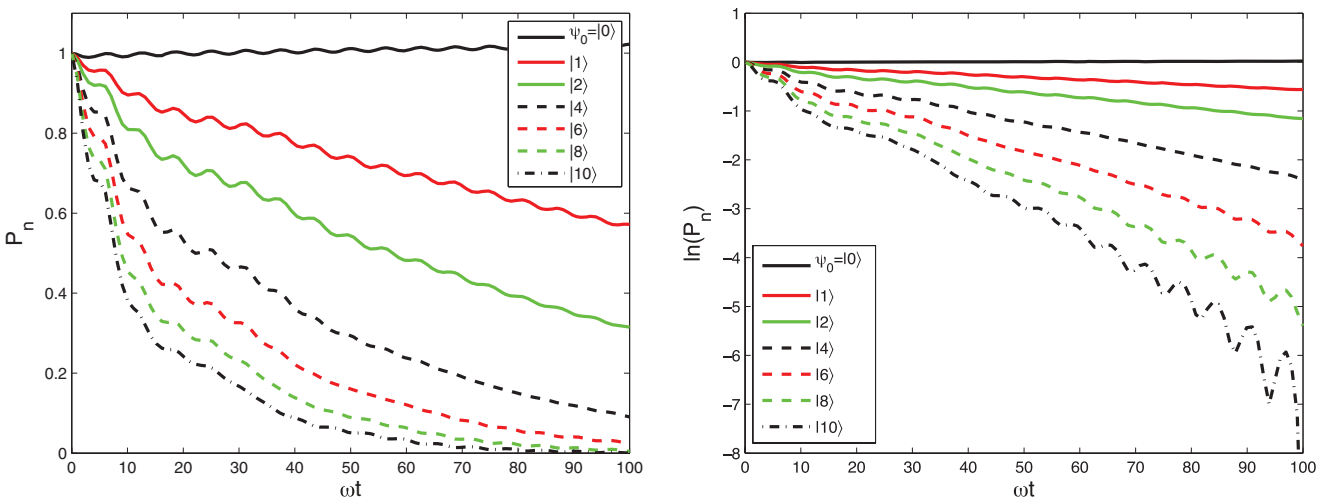

FIG. 11. (Color online) Left: P_n vs ωt for a resonator coupled to six noninteracting TLS's. Right: $\ln(P)_n$ vs ωt. For all curves, $T_1 = 10$.

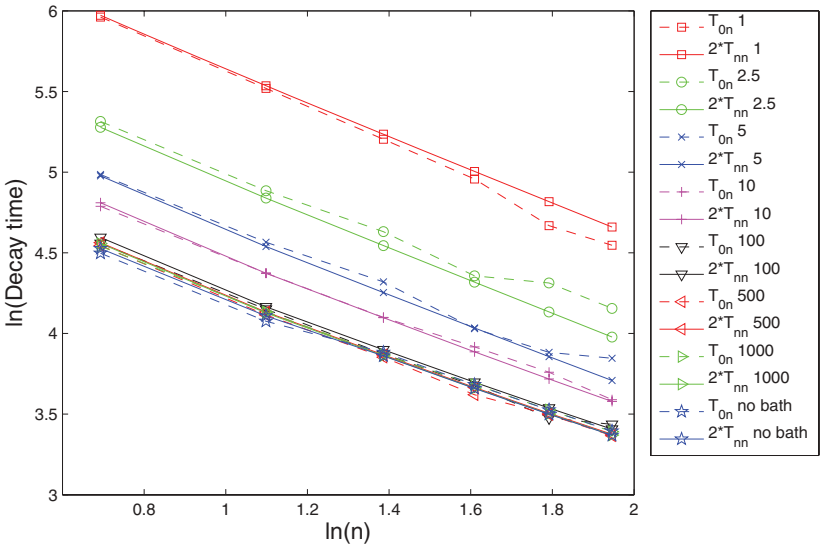

FIG. 12. (Color online) T_{0n} and $2T_{nn}$ for the initial superposition state $|\psi_0\rangle = 1/\sqrt{2}(|0\rangle + |n\rangle)$ with a range of T_1 values shown in the legend. In particular, T_1 ranges from 1 to 1000, while "no bath" denotes that the TLS's are undamped. The observed trend for a given n is decreasing decay time with increasing T_1. For all curves, the resonator is coupled to six noninteracting TLS's.

We then make a rotating wave and a Markov approximation, and we assume temperatures $k_B T \ll E^{(\alpha)}$ such that $\langle \sigma_z^{(\alpha)} \rangle \approx 1$ and the longitudinal contribution depending on $\cos\theta^{(\alpha)}$ is suppressed, leaving only the transverse contributions depending on $\sin\theta^{(\alpha)}$. We thus obtain the probability that the mechanical resonator is in the nth Fock state, $P_n = \langle n|\rho_m|n\rangle$:

$$\frac{dP_n(t)}{dt} = -\gamma_{\text{Fock}}\left[nP_n(t) - (n+1)P_{n+1}(t)\right], \tag{12}$$

where $\gamma_{\text{Fock}}(\equiv T_{11}^{-1})$ gives the decay rate for an initial $n = 1$ Fock state:

$$\gamma_{\text{Fock}} = -\frac{1}{\hbar^2}\sum_{\alpha=1}^{N}(\lambda^{(\alpha)})^2 \sin^2\theta^{(\alpha)} \frac{2\Gamma_2^{(\alpha)}}{\left(\Gamma_2^{(\alpha)}\right)^2 + (E^{(\alpha)}/\hbar - \omega_m)^2}. \tag{13}$$

Equation (12) shows that the decay rate for an initial n Fock state scales with n, as we saw in the numerical simulations. The dependence of the probability decay rate on T_1 comes from the TLS dephasing rate $\Gamma_2^{(\alpha)}$ dependence of the Lorentzian term.

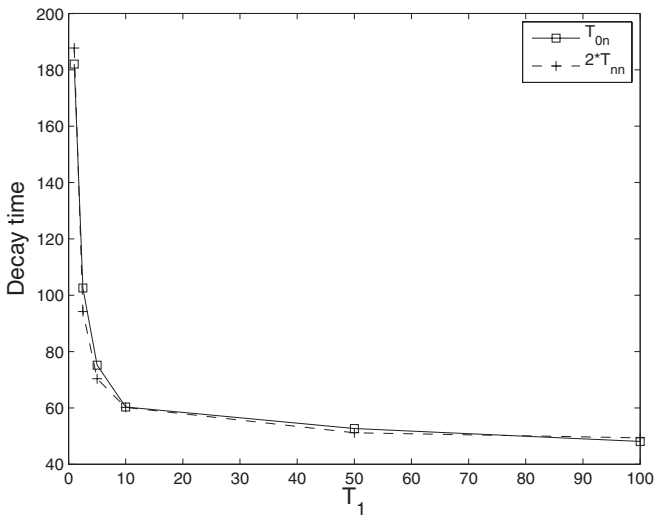

FIG. 13. $2T_{nn}$ and T_{0n} vs T_1 for the $n = 4$ superposition state.

From Eq. (10), we see that $\Gamma_2^{(\alpha)}$ scales as $\Gamma_1^{(\alpha)}$. We now consider the form of the given Lorentzian, subject to the rescaling ϵT_1:

$$\frac{2\Gamma_2/\epsilon}{(\Gamma_2/\epsilon)^2 + (E/\hbar - \omega_m)^2}. \tag{14}$$

Figure 15 shows the Lorentzian factor as a function of ω_m for three different ϵ values. As we increase ϵ (i.e., increase the TLS damping time, T_1), the Lorentzian factor correspondingly increases, as long as $|E/\hbar - \omega_m| < \Gamma_2/\epsilon$, i.e., within the Lorentzian linewidth. Physically, Eq. (13) indicates that for a mechanical resonator that is approximately resonant with a TLS, the longer the TLS decay time, the more rapidly it absorbs energy from the mechanical resonator, and hence the shorter the Fock state probability decay time. However, as ϵ continues to increase, we eventually have that $|E/\hbar - \omega_m| > \Gamma_2/\epsilon$. The TLS is no longer approximately resonant with the oscillator, and so the Lorentzian factor and thus the decay rate decreases. Figure 16 shows the dependence of the decay time on ϵ that follows from one of the distributions

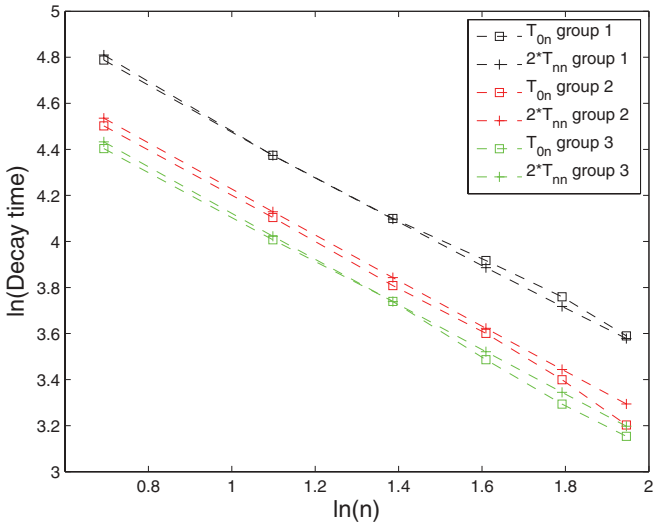

FIG. 14. (Color online) $2T_{nn}$ and T_{0n} vs n for three different realizations of the TLS parameters. For all curves, $T_1 = 10$.

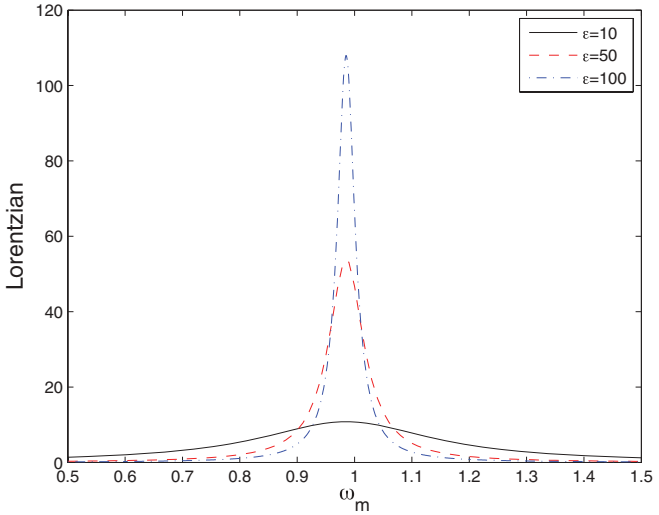

FIG. 15. (Color online) Lorentzian function vs ω_m for three different ϵ values. TLS parameters are $\Delta_0 = 0.6281$, $\Delta_b = 0.7592$, and $T_1 = 0.6396$.

of TLS-oscillator coupling and parameter values used in the numerical simulations. The intermediate dip is due to some of the TLS's going out of resonance. While the plot does not show quite the same monotonically decreasing decay time with increasing ϵ as found in the numerical simulation, it does give approximately the same overall decreasing trend. Differences are due to the breakdown of the Born-Markov approximation for treating the TLS subsystem as a bath.

IV. TLS-TLS INTERACTIONS

A. Derivation of the Hamiltonian

Experiments have shown that interactions between TLS's play an important role in dissipation and decoherence.[4,6,7] In this section, we derive the TLS-TLS interaction Hamiltonian. We begin with the Hamiltonian for an elastic wave system interacting with TLS defects. The Lagrangian for an elastic

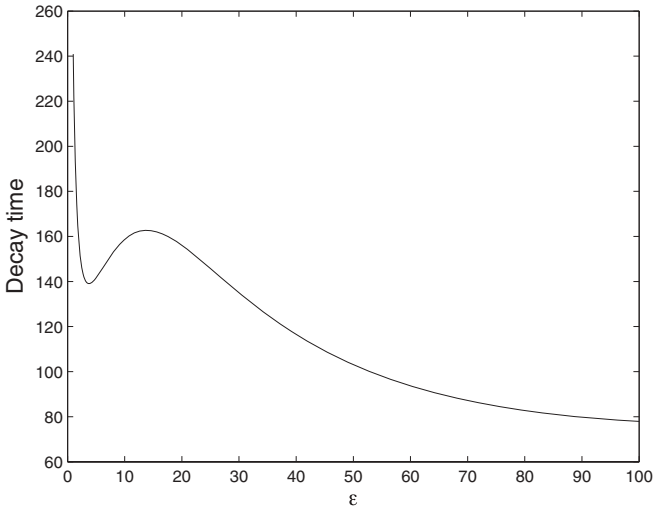

FIG. 16. Fock state decay time vs TLS T_1 scaling factor ϵ for the $n = 1$ Fock state.

wave system is[31]

$$L_{\text{wave}} = \frac{1}{2}\int_V d^3r[\rho\dot{u}_i(\vec{r},t)\dot{u}_i(\vec{r},t) - c_{ijkl}\partial_i u_j(\vec{r},t)\partial_k u_l(\vec{r},t)], \tag{15}$$

where V is the system volume, ρ is the mass density, $u_i(\vec{r},t)$, $i = 1,2,3$ is the ith component of the displacement vector field, and c_{ijkl} is the elastic modulus tensor. We use the Einstein summation convention. The Hamiltonian is by definition

$$H_{\text{wave}} = \dot{u}_i\frac{\partial L_{\text{wave}}}{\partial\dot{u}_i} - L_{\text{wave}}, \tag{16}$$

which, with Eq. (15), gives

$$H_{\text{wave}} = \int_V d^3r\left[\frac{\rho}{2}\dot{u}_i\dot{u}_i + \frac{1}{2}c_{ijkl}\partial_i u_j\partial_k u_l\right]. \tag{17}$$

In addition to the noninteracting TLS Hamiltonian (1), we have the TLS-wave system interaction Hamiltonian

$$H_{\text{int}} = -\sum_{\alpha=1}^{N}\left[v_{ij}^{(\alpha)}\epsilon_{ij}^{(\alpha)}\sigma_z^{(\alpha)}\right], \tag{18}$$

where $v_{ij}^{(\alpha)}$ is the deformation potential tensor at the α TLS location $\vec{r}^{(\alpha)}$ and

$$\epsilon_{ij}^{(\alpha)} = \tfrac{1}{2}[\partial_i u_j(\vec{r}^{(\alpha)},t) + \partial_j u_i(\vec{r}^{(\alpha)},t)] \tag{19}$$

is the strain tensor at $\vec{r}^{(\alpha)}$. Since $v_{ij}^{(\alpha)} = v_{ji}^{(\alpha)}$, we can rewrite the interaction Hamiltonian as

$$H_{\text{int}} = -\sum_{\alpha=1}^{N}\left[v_{ij}^{(\alpha)}\partial_i u_j(\vec{r}^{(\alpha)},t)\sigma_z^{(\alpha)}\right]. \tag{20}$$

The full Hamiltonian is now

$$\begin{aligned} H = &\int_V d^3r\left[\frac{\rho}{2}\dot{u}_i\dot{u}_i + \frac{1}{2}c_{ijkl}\partial_i u_j\partial_k u_l\right] \\ &+\sum_{\alpha=1}^{N}\left[\frac{1}{2}\Delta_0^{(\alpha)}\sigma_z^{(\alpha)} + \frac{1}{2}\Delta_b^{(\alpha)}\sigma_x^{(\alpha)}\right] \\ &-\sum_{\alpha=1}^{N}\left[v_{ij}^{(\alpha)}\partial_i u_j(\vec{r}^{(\alpha)},t)\sigma_z^{(\alpha)}\right]. \end{aligned} \tag{21}$$

For weak TLS-wave system interactions, we can in principle start with this Hamiltonian and derive a master equation for the observed flexural wave mode of interest that interacts with the N TLS's. The rest of the elastic wave normal modes then form the TLS bath, as well as mediate the interactions between the TLS's. Instead, we will adopt a less rigorous approach to derive the approximate form of the elastic wave-induced interaction between any pair of TLS's. We assume that the time scale for the phonon mediated interaction between two TLS's is much shorter than their internal dynamics time scale; the two TLS's are therefore approximated as "frozen," with each in a given spin state. We take as our starting point the following Hamiltonian for the interaction between two TLS's without

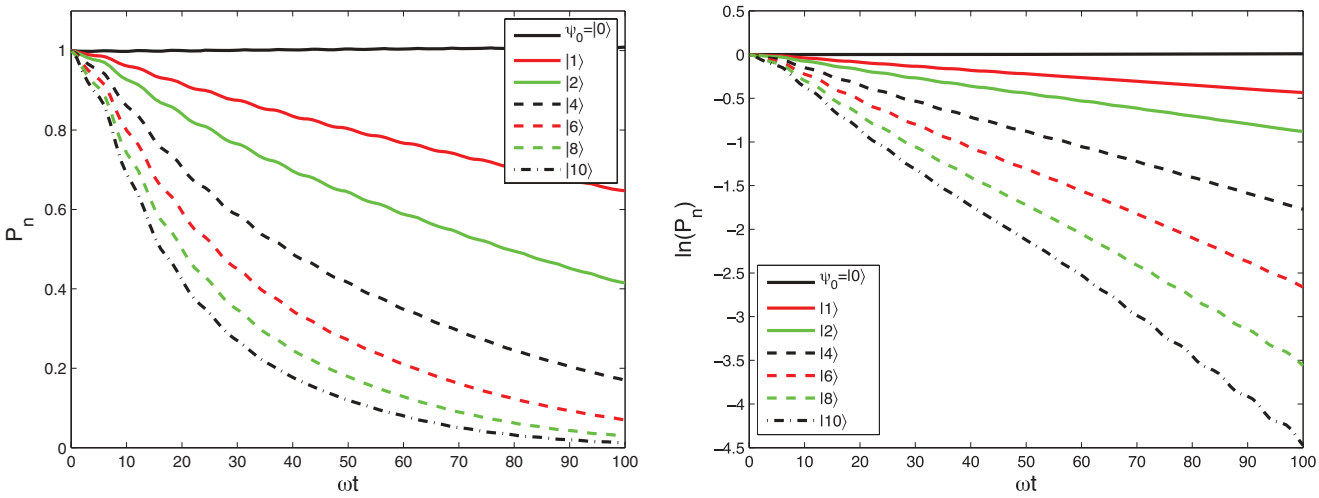

FIG. 17. (Color online) Left: P_n vs ωt for a resonator coupled to three interacting TLS's. Right: $\ln(P_n)$ vs ωt. For all curves, $T_1 = 10$.

the noninteracting TLS part:

$$H_{\text{approx2TLS}} = \int_V d^3r \left[\frac{\rho}{2}\dot{u}_i\dot{u}_i + \frac{1}{2}c_{ijkl}\partial_i u_j \partial_k u_l - \sum_{\alpha=1}^{2} v_{ij}^{(\alpha)} \partial_i u_j(\vec{r}^{(\alpha)},t)\sigma_z^{(\alpha)}\delta(\vec{r}-\vec{r}^{(\alpha)}) \right]. \quad (22)$$

Next, we express this approximate Hamiltonian operator at $t = 0$ in terms of the normal mode, phonon creation, and annihilation operators. We define

$$u_i(\vec{r},0) = \sum_\beta \sqrt{\frac{\hbar}{2\rho\omega_\beta}} [a_\beta u_{\beta,i}(\vec{r}) + a_\beta^\dagger u_{\beta,i}^*(\vec{r})] \quad (23)$$

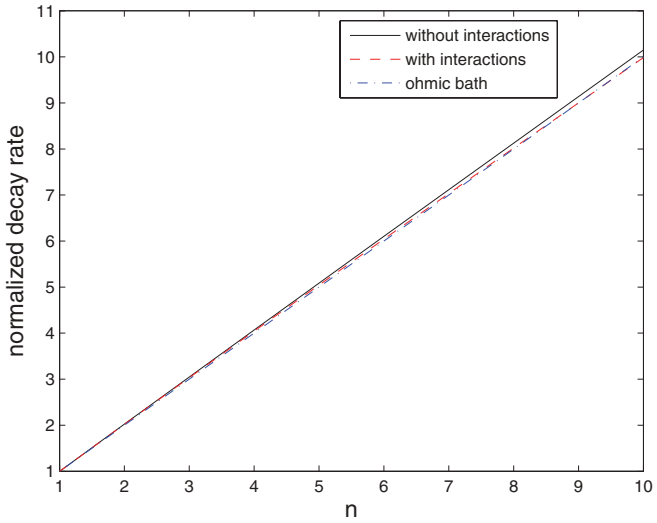

FIG. 18. (Color online) Normalized decay rate vs n for single Fock states. The resonator is coupled to three noninteracting TLS's (solid), three interacting TLS's (dash), and to an Ohmic bath (dot-dash). For all curves, $T_1 = 10$.

and

$$\dot{u}_i(\vec{r},0) = -i \sum_\beta \sqrt{\frac{\hbar\omega_\beta}{2\rho}} [a_\beta u_{\beta,i}(\vec{r}) - a_\beta^\dagger u_{\beta,i}^*(\vec{r})], \quad (24)$$

where $[a_\beta, a_{\beta'}^\dagger] = \delta_{\beta,\beta'}$, with β denoting the normal mode. The normal modes are solutions to

$$c_{ijkl}\partial_j\partial_k u_{\beta,l} = -\rho\omega_\beta^2 u_{\beta,i}. \quad (25)$$

Substituting Eqs. (23) and (24) into Eq. (22) and using Eq. (25) and the orthonormality and completeness relations

$$\int_V d^3r u_{\beta,i}(\vec{r}) u_{\beta',i}^*(\vec{r}) = \delta_{\beta,\beta'} \quad (26)$$

and

$$\sum_\beta u_{\beta,i}(\vec{r}) u_{\beta,j}^*(\vec{r}') = \delta_{ij}\delta(\vec{r}-\vec{r}'), \quad (27)$$

respectively, we obtain

$$H_{\text{approx2TLS}} = \sum_\beta \left[\frac{\hbar\omega_\beta}{2}(a_\beta a_\beta^\dagger + a_\beta^\dagger a_\beta) + f_\beta a_\beta + f_\beta^\dagger a_\beta^\dagger \right], \quad (28)$$

where f_β is defined as

$$f_\beta = \sqrt{\frac{\hbar}{2\rho\omega_\beta}} \int_V d^3r u_{\beta,i}(\vec{r}) v_{ij} \times \left[\partial_j \delta(\vec{r}-\vec{r}^{(1)})\sigma_z^{(1)} + \partial_j\delta(\vec{r}-\vec{r}^{(2)})\sigma_z^{(2)} \right]. \quad (29)$$

Making the substitution $a_\beta = b_\beta + c_\beta$, we obtain

$$H_{\text{approx2TLS}} = \sum_\beta \left[\frac{\hbar\omega_\beta}{2}(b_\beta b_\beta^\dagger + b_\beta^\dagger b_\beta) + \hbar\omega_\beta(c_\beta^\dagger b_\beta + c_\beta b_\beta^\dagger) + f_\beta b_\beta + f_\beta^\dagger b_\beta^\dagger + c_\beta f_\beta + c_\beta^\dagger f_\beta^\dagger + \hbar\omega_\beta c_\beta c_\beta^\dagger \right]. \quad (30)$$

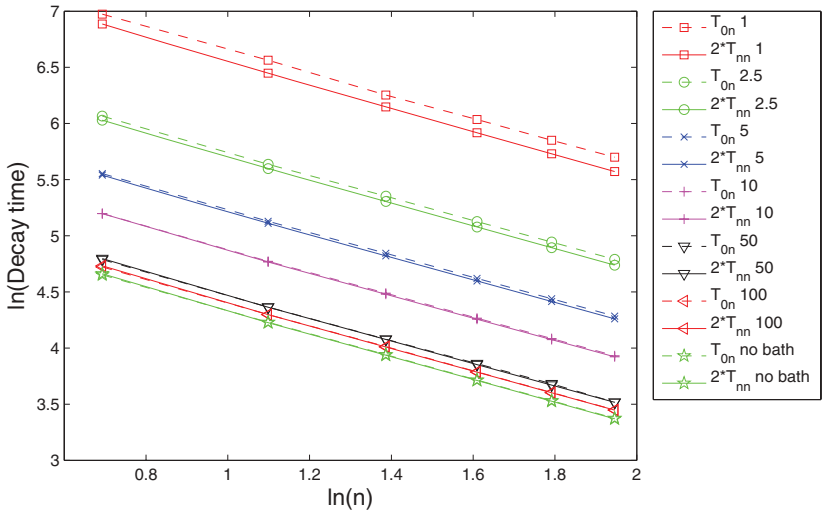

FIG. 19. (Color online) T_{0n} and T_{nn} for the initial superposition state $|\psi_0\rangle = 1/\sqrt{2}(|0\rangle + |n\rangle)$ with a range of T_1 values shown in the legend. In particular, T_1 ranges from 1 to 100, while "no bath" denotes that the TLS's are undamped. The observed trend for a given n is decreasing decay time with increasing T_1. For all curves, the resonator is coupled to three interacting TLS's.

Defining $c_\beta = -f_\beta^\dagger/\hbar\omega$ and $c_\beta^\dagger = -f_\beta/\hbar\omega$, we see that the mixed operator terms in Eq. (30) cancel out, and we have

$$H_{\text{approx2TLS}} = \sum_\beta \left[\frac{\hbar\omega_\beta}{2}(b_\beta b_\beta^\dagger + b_\beta^\dagger b_\beta) - \frac{f_\beta f_\beta^\dagger}{\hbar\omega}\right]. \tag{31}$$

The TLS-TLS interaction term we are seeking is contained within the quadratic f-term in Eq. (31). Substituting in Eq. (29) and simplifying, we obtain the following for the TLS-TLS interaction:

$$H_{\text{TLS-TLS}} = -\sigma_z^{(1)}\sigma_z^{(2)}\nu_{ik}\nu_{jl}\frac{1}{\rho}\sum_\beta \frac{1}{\omega_\beta^2}\partial_k u_{\beta,i}(\vec{r}^{(1)})\partial_l u^*_{\beta,j}(\vec{r}^{(2)}), \tag{32}$$

where we have neglected TLS self-interaction terms.

The strength of the interaction between the two TLS's will depend on the nature of the elastic medium in which the TLS's are embedded, as expressed by the mode sum in Eq. (32). Let us now try to come up with a simple semiquantitative approximation to the mode sum part in the interaction term (32) using dimensional analysis. From the completeness relation (27), the displacement mode function $u_{\beta,i}$ has the dimensions $L^{-3/2}$ in terms of some to-be-determined length scale L. The mode frequency depends on the speed of sound v, and so scales as $\omega_\beta \sim v/L$. Thus, the overall length dimension for the mode sum in Eq. (32) is L^{-3}. The relevant length scale, however, depends on the geometry of the embedding elastic medium. For a bulk, three-dimensional (3D) medium where the two TLS's are far from any of the medium boundaries, the appropriate length scale must be the separation r_{12} between the two TLS's. Thus, for a 3D medium we have

$$H_{2\text{TLS}}^{\text{3D}} \sim \sigma_z^{(1)}\sigma_z^{(2)}\frac{v^2}{\rho v^2}\frac{1}{r_{12}^3}, \tag{33}$$

where we have neglected the anisotropy of the deformation potential. For a membranelike elastic medium, where the separation between the two TLS's is large compared to the membrane thickness d, we must lose one of the r_{12} factors in Eq. (33), to be replaced by d. Thus, for an effectively 2D medium, we have

$$H_{2\text{TLS}}^{\text{2D}} \sim \sigma_z^{(1)}\sigma_z^{(2)}\frac{v^2}{\rho v^2 d}\frac{1}{r_{12}^2}. \tag{34}$$

Finally, for a wirelike elastic medium where the separation between the two TLS's is large compared to the wire's cross-sectional dimensions d and w, we must lose two of the r_{12} factors in Eq. (33). Thus, for an effectively 1D medium, we have

$$H_{2\text{TLS}}^{\text{1D}} \sim \sigma_z^{(1)}\sigma_z^{(2)}\frac{v^2}{\rho v^2 d w}\frac{1}{r_{12}}. \tag{35}$$

Note that, as the dimensions of the elastic structure are reduced, the TLS-TLS interaction becomes longer-ranged. In particular, for a wirelike structure, the reduced volume and hence reduced number of TLS's will in part be compensated by a longer-ranged interaction.

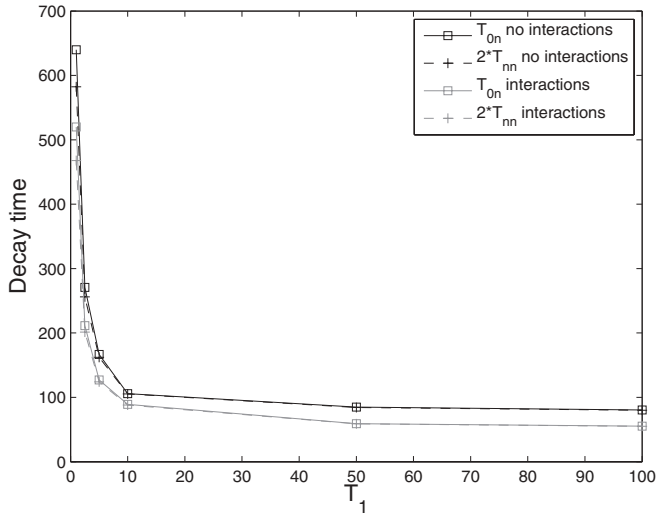

FIG. 20. T_{nn} and T_{0n} vs T_1 for the $n = 4$ superposition state. The resonator is coupled to three noninteracting (black) and three interacting (gray) TLS's.

B. Three interacting TLS's

We now include TLS-TLS interactions. We group all variables in Eq. (32) except the σ operators into a single variable,

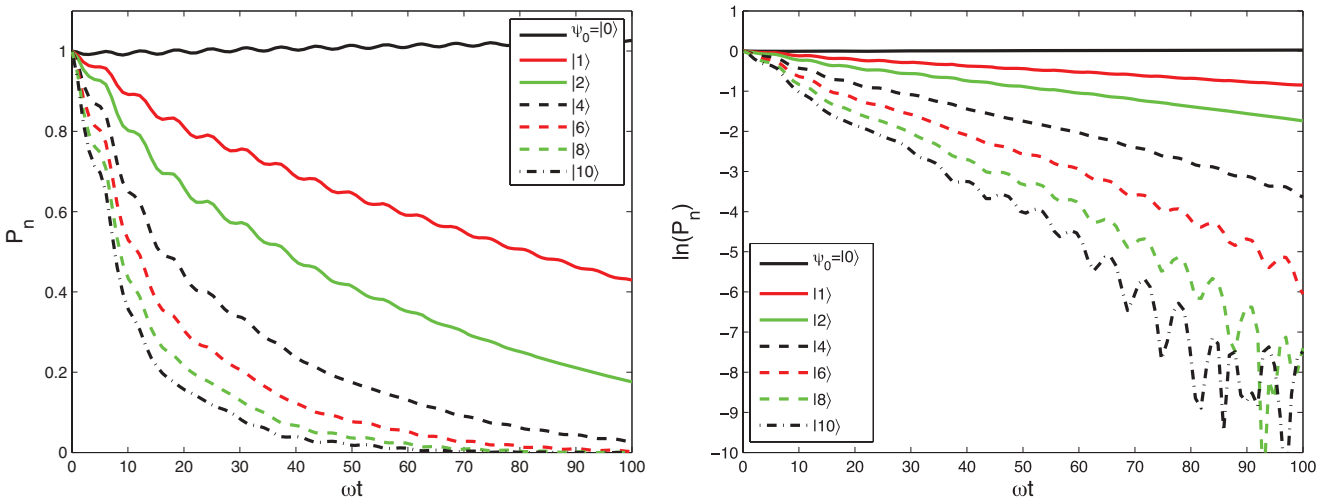

FIG. 21. (Color online) Left: P_n vs ωt for a resonator coupled to six interacting TLS's. Right: $\ln(P)_n$ vs ωt. For all curves, $T_1 = 10$.

$\zeta^{(\alpha\beta)}$, simplifying the TLS-TLS interaction Hamiltonian to

$$H_{\text{TLS-TLS}} = -\sigma_z^{(\alpha)}\sigma_z^{(\beta)}\zeta^{(\alpha\beta)}. \tag{36}$$

For the plots in this section and the next, we choose a value for ζ and then generate a random $\zeta^{(\alpha\beta)}$ within $\pm 50\%$ of this value for each pair of TLS's. Unless otherwise specified, the values are centered around $\zeta = 0.1/6$. This interaction strength is somewhat larger than estimates based on Eq. (35), chosen to be comparable to the resonator-TLS coupling strength λ so as to resolve the effects of including the TLS-TLS interactions. We plot P_n versus ωt for a resonator coupled to three interacting TLS's.

Figure 17 shows that P_n decays exponentially as a function of time, and we again apply a linear fit to the log plot to extract a decay rate. In Fig. 18, we plot the normalized decay rate for a resonator coupled to three noninteracting TLS's (solid), to three interacting TLS's (dash), and to an Ohmic bath (dot-dash). The dot-dashed and dashed curves are practically indistinguishable, suggesting that the addition of TLS-TLS interactions allows the three TLS's to absorb energy like an Ohmic bath, even for higher-n Fock states.

We now investigate the decay of a superposition state. Figure 19 shows the on- and off-diagonal decay times T_{0n} and $2T_{nn}$ as a function of n for a range of TLS T_1 values. As in the case of three noninteracting TLS's, the curves have slopes ≈ -1 and also $T_{0n} \approx 2T_{nn}$; dephasing is negligible.

Figure 20 shows the T_1 dependence of the on- and off-diagonal decay times for a resonator coupled to three noninteracting (black) and three interacting (gray) TLS's. The decay times are reduced for the resonator coupled to interacting TLS's, with the same unexpected T_1 dependence as noted in the preceding section.

C. Six interacting TLS's

We now couple the resonator to six interacting TLS's. Figure 21 shows the number state probability as a function of time for a resonator coupled to six damped, interacting TLS's. The shape of the curves is similar to that for six noninteracting TLS's, with the log plot appearing approximately linear. Again, the oscillations appearing in the larger n curves at long times are numerical artifacts due to the exponentially small decay probabilities. In Fig. 22, we plot the decay rate as a function of n for six TLS's with (dash) and without (solid) TLS-TLS interactions, and for a resonator coupled only to an Ohmic bath (dot-dash). We note that the decay is similar for the two cases with slope close to 1.

Next we study the T_1 dependence of the on- and off-diagonal terms of the density matrix for a superposition of Fock states, as we did in Fig. 20. Figure 23 shows T_{nn} and T_{0n} as a function of T_1 for the $n = 4$ superposition state for a resonator coupled to six noninteracting (black) and six interacting (gray) TLS's. The plot shows that in both cases, a reduction of T_1 causes an increase in the decay time of the on- and off-diagonal terms. As

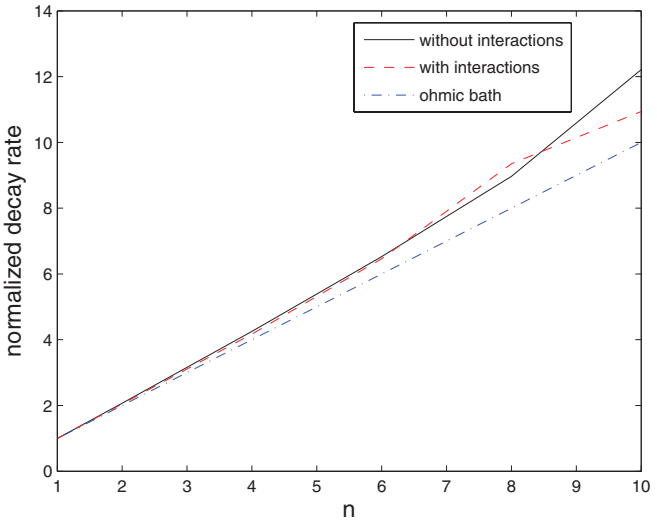

FIG. 22. (Color online) Normalized decay rate vs n for a single Fock state. The resonator is coupled to six noninteracting TLS's (solid), six interacting TLS's (dash), and to an Ohmic bath (dot-dash). For all curves, $T_1 = 10$.

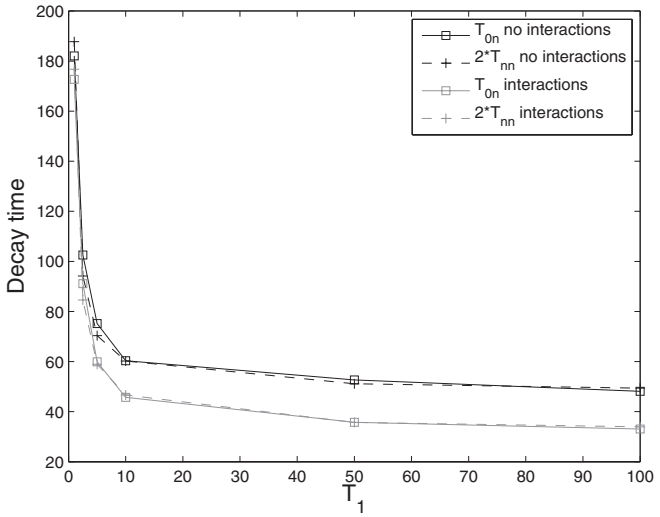

FIG. 23. T_{nn} and T_{0n} vs T_1 for the $n = 4$ superposition state. The resonator is coupled to six noninteracting (black) and six interacting (gray) TLS's.

for the three interacting TLS's case, the addition of TLS-TLS interactions decreases the decay times.

Lastly, we plot T_{nn} and T_{0n} as a function of the TLS-TLS coupling parameter ζ. Figure 24 shows the ζ dependence of the decay times for two different sets of random $\zeta^{(\alpha\beta)}$. In both cases, the decay time of the diagonal terms, T_{nn}, shows a linear dependence on the strength of the TLS-TLS coupling, with a slight variation in the slope for the two realizations. The off-diagonal terms, particularly for the second group of random $\zeta^{(\alpha\beta)}$ values, decay less uniformly with respect to ζ, but the overall behavior shows a clear dependence on ζ, with stronger TLS-TLS coupling leading to faster decay of both the diagonal and off-diagonal terms of the density matrix.

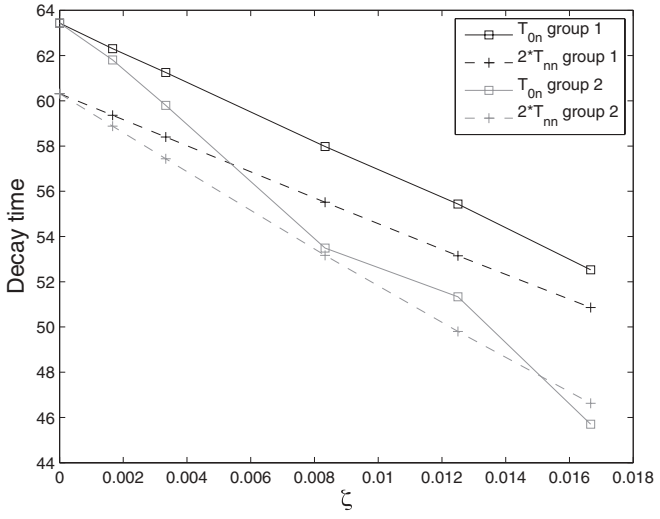

FIG. 24. T_{nn} and T_{0n} vs the TLS-TLS interaction strength ζ for two different realizations of the random $\zeta^{(ij)}$ values. The resonator is initially in the $n = 4$ superposition state. For all curves, $T_1 = 10$.

V. CONCLUSION

In this work, we have explored the effects of near-resonant TLS's on the decay of initial Fock states and their superpositions for a mechanical oscillator at low temperatures. We began our investigation with an oscillator coupled to a single TLS, then we increased the number to three, and then six TLS's. For initial Fock states $|n\rangle$ of an oscillator coupled to a single, damped TLS, we observed oscillatory decay with a rate that appeared to decrease with increasing n. In contrast, for an oscillator coupled to three TLS's, we found that Fock states and Fock state superpositions decayed monotonically, similar to that due to an Ohmic oscillator bath. In particular, the decay rate T_{nn}^{-1} of the initial Fock state $|n\rangle$ scaled closely as n, while the interference terms of the Fock state superposition $|0\rangle + |n\rangle$ decayed close to twice as slowly, $T_{0n} \approx 2T_{nn}$, approximately coinciding with the Fock state decay behavior of an oscillator system coupled to a bath of free oscillators with Ohmic spectral density. We noted that there was some variation in the Fock state decay times for different realizations of the random TLS variables, reflecting the fact that we were intermediate between a single TLS and a dense spectrum of TLS's. For an oscillator coupled to six TLS's, we continued to find an Ohmic-like decay dependence, while the variation in the decay for different random TLS realizations was less than for the three-TLS's case.

The mechanical resonator Fock state decay rates showed an unexpected dependence on the TLS relaxation time T_1, in particular increasing with increasing T_1. The analysis based on the Born approximation in the resonator-TLS coupling in Sec. III D suggested a possible explanation in terms of the T_1 dependences of the TLS decay linewidths. However, the Born approximation breaks down in the limiting case $T_1 \to \infty$, and hence it cannot explain how the effectively Ohmic oscillator bath decay behavior is maintained even when the mechanical resonator is coupled to as few as three undamped TLS's. As stated in the Introduction, the latter behavior is reminiscent of subsystem thermalization of closed, interacting many-body systems.[27] We shall explore this connection further in a future publication.

Including strain-mediated pair interactions between the TLS's serves to enhance the Fock state decay rates while maintaining the Ohmic-like decay behavior. We noted that the strain-mediated pair interactions are longer-ranged in reduced dimensional systems. Thus, while there will be fewer TLS's near resonance in a vibrating nanowire as compared with a bulk mechanical resonator of the same material, we might expect that the longer-ranged TLS-TLS interactions in the former system will partly compensate by limiting the Fock state lifetimes.

This work highlights the need for analytical approximations in order to understand the numerical results. One possible starting point is to assume the rotating wave approximation for the oscillator-TLS Hamiltonian (2), giving the Tavis-Cummings Hamiltonian with randomly distributed TLS energies and couplings. We can then apply a polaronlike unitary transformation to decouple the oscillator from the TLS's.[32] Evidentally, the numerical simulations presented here can serve as a useful check for the validity of possible analytical approximations. Given the established validity of an approximation method,

one can then go beyond the small TLS number limitation of computational methods to account also for lower-energy TLS defects in the mechanical resonator. Such far-from-resonant TLS's are responsible for $1/f$ noise, resulting in shorter off-diagonal $T_{0n} < 2T_{nn}$ decay times [through the longitudinal $\cos\theta^{\alpha}$ contribution in the Born approximated Eq. (8)].[11] Much work remains to be done to understand the quantum-classical correspondence for nanomechanical resonators interacting with tunneling TLS defects at low temperatures, particularly now that experiments demonstrating such systems in the quantum limit are becoming a reality.

ACKNOWLEDGMENTS

We thank Andrew Armour, Lin Tian, and Ignacio Wilson-Rae for helpful discussions. We also thank Susan Schwarz for her assistance in implementing the numerical simulations on Dartmouth's Discovery Cluster. This work was supported by the National Science Foundation under Grants No. DMR-0804477 and No. DMR-1104790.

[1] A. D. O'Connell, M. Hofheinz, M. Ansmann, R. C. Bialczak, M. Lenander, E. Lucero, M. Neeley, D. Sank, H. Wang, M. Weides, J. Wenner, J. M. Martinis, and A. N. Cleland, Nature (London) **464**, 697 (2010).

[2] P. W. Anderson, B. I. Halperin, and C. M. Varma, Philos. Mag. **25**, 1 (1972).

[3] W. A. Phillips, J. Low Temp. Phys. **7**, 351 (1972).

[4] W. Arnold and S. Hunklinger, Solid State Commun. **17**, 883 (1975).

[5] B. Golding, J. E. Graebner, and R. J. Schutz, Phys. Rev. B **14**, 1660 (1976).

[6] W. Arnold, C. Martinon, and S. Hunklinger, J. Phys. (Paris) Colloq. **39**, C6-961 (1978).

[7] J. E. Graebner and B. Golding, Phys. Rev. B **19**, 964 (1979).

[8] *Tunneling Systems in Amorphous and Crystalline Solids*, edited by P. Esquinazi (Springer-Verlag, Berlin, 1998).

[9] R. W. Simmonds, K. M. Lang, D. A. Hite, S. Nam, D. P. Pappas, and J. M. Martinis, Phys. Rev. Lett. **93**, 077003 (2004).

[10] L.-C. Ku and C. C. Yu, Phys. Rev. B **72**, 024526 (2005).

[11] A. Shnirman, G. Schön, I. Martin, and Y. Makhlin, Phys. Rev. Lett. **94**, 127002 (2005).

[12] J. M. Martinis, K. B. Cooper, R. McDermott, M. Steffen, M. Ansmann, K. D. Osborn, K. Cicak, S. Oh, D. P. Pappas, R. W. Simmonds, and C. C. Yu, Phys. Rev. Lett. **95**, 210503 (2005).

[13] L. Tian and R. W. Simmonds, Phys. Rev. Lett. **99**, 137002 (2007).

[14] M. Neeley, M. Ansmann, R. C. Bialczak, M. Hofheinz, N. Katz, E. Lucero, A. O'Connell, H. Wang, A. N. Cleland, and J. M. Martinis, Nat. Phys. **4**, 523 (2008).

[15] A. D. O'Connell, M. Ansmann, R. C. Bialczak, M. Hofheinz, N. Katz, E. Lucero, C. McKenney, M. Neeley, H. Wang, E. M. Weig, A. N. Cleland, and J. M. Martinis, Appl. Phys. Lett. **92**, 112903 (2008).

[16] Z. Kim, V. Zaretskey, Y. Yoon, J. F. Schneiderman, M. D. Shaw, P. M. Echternach, F. C. Wellstood, and B. S. Palmer, Phys. Rev. B **78**, 144506 (2008).

[17] M. Constantin, C. C. Yu, and J. M. Martinis, Phys. Rev. B **79**, 094520 (2009).

[18] J. Lisenfeld, C. Müller, J. H. Cole, P. Bushev, A. Lukashenko, A. Shnirman, and A. V. Ustinov, Phys. Rev. Lett. **105**, 230504 (2010).

[19] J. H. Cole, C. Müller, P. Bushev, G. J. Grabovskij, J. Lisenfeld, A. Lukashenko, A. V. Ustinov, and A. Shnirman, Appl. Phys. Lett. **97**, 252501 (2010).

[20] O. Arcizet, R. Rivière, A. Schliesser, G. Anetsberger, and T. J. Kippenberg, Phys. Rev. A **80**, 021803(R) (2009).

[21] A. Venkatesan, K. J. Lulla, M. J. Patton, A. D. Armour, C. J. Mellor, and J. R. Owers-Bradley, Phys. Rev. B **81**, 073410 (2010).

[22] F. Hoehne, Yu. A. Pashkin, O. Astafiev, L. Faoro, L. B. Ioffe, Y. Nakamura, and J. S. Tsai, Phys. Rev. B **81**, 184112 (2010).

[23] J. Sulkko, M. Sillanpää, P. Häkkinen, L. Lechner, M. Helle, A. Fefferman, J. Parpia, and P. J. Hakonen, Nano Lett. **10**, 4884 (2010).

[24] R. Rivière, S. Deléglise, S. Weis, E. Gavartin, O. Arcizet, A. Schliesser, and T. J. Kippenberg, Phys. Rev. A **83**, 063835 (2011).

[25] L. G. Remus, M. P. Blencowe, and Y. Tanaka, Phys. Rev. B **80**, 174103 (2009).

[26] G. D. Cole, I. Wilson-Rae, K. Werbach, M. R. Vanner, and M. Aspelmeyer, Nat. Commun. **2**, 231 (2011).

[27] A. Polkovnikov, K. Sengupta, A. Silva, and M. Vengalattore, Rev. Mod. Phys. **83**, 863 (2011).

[28] S. Tan, *Quantum Optics Toolbox*, http://qo.phy.auckland.ac.nz/toolbox/.

[29] N. Lu, Phys. Rev. A **40**, 1707 (1989).

[30] W. B. Case, Am. J. Phys. **76**, 937 (2008).

[31] N. Ashcroft and N. D. Mermin, in *Solid State Physics* (Holt, Rinehart, and Winston, New York, 1976), p. 446.

[32] L. Tian, Phys. Rev. B **84**, 035417 (2011).